Dual-frequency Doppler-free spectroscopy for simultaneous laser stabilization in compact atomic physics experiments

Nathan Cooper,[1,*] Somaya Madkhaly,[1,2] David Johnson,[1] Benjamin Hopton,[1] Daniele Baldolini,[1] and Lucia Hackermüller[1]
[1]*School of Physics and Astronomy, University of Nottingham, University Park, Nottingham NG7 2RD, United Kingdom*
[2]*Department of Physics, Jazan University, Jazan 45142, Kingdom of Saudi Arabia*

(Received 16 December 2022; revised 9 June 2023; accepted 26 June 2023; published 31 July 2023)

Vapor-cell spectroscopy is an essential technique in many fields and is particularly relevant for quantum technologies. Most atom- and ion-trapping experiments rely on simultaneous spectroscopy of two atomic transitions, employing a separate apparatus for each transition. We demonstrate simultaneous spectroscopy on two atomic transitions, within a single apparatus, using spatially overlapped beams from two independent lasers. This method enables compact setups and offers superior spectroscopic performance, leading to sharper spectroscopy peaks, stronger absorption signals, and superior laser stability. Doppler-free locking features become accessible over a frequency range several hundred megahertz wider than for standard saturated absorption spectroscopy. Exploring the full parameter space associated with dual-frequency spectroscopy reveals a latticelike structure of sharp resonance features, which enhances experimental versatility by allowing laser frequency stabilization within a wide manifold of locations in two-dimensional frequency space. We present data for ^{133}Cs and ^{85}Rb and compare our results to a theoretical model. Employing the technique for frequency stabilization close to the D_2 line of ^{85}Rb results in an improvement in frequency stability by a factor typically between 2 and 3 for averaging times of up to 1 s. The technique will advance portable quantum technologies and facilitate high-precision measurements.

DOI: 10.1103/PhysRevA.108.013521

I. INTRODUCTION

The last decade has seen an explosion of interest in quantum technologies and experiments that exploit the coherent interaction of atoms with frequency-stabilized laser radiation. This includes not only growth in laboratory-based precision experiments [1–3] but also ambitious proposals to test key aspects of fundamental physics using space-based apparatus [4–7] and distributed atomic sensor networks [8]; these rely on precise laser frequency stabilization. At the same time, the quantum technology sector is finding highly important, real-world applications for atomic physics techniques in areas such as subterranean mapping, inertial navigation, and medical imaging [9–14], resulting in the need for compact and robust systems. Typically, at least two independent lasers are required, as light resonant with two different atomic transitions, referred to as the "cooler" and "repumper" transitions, is essential [15].

Herein, we demonstrate simultaneous frequency stabilization of two lasers using a single spectroscopic setup, achieving superior frequency stability compared to standard techniques while at the same time reducing the size and complexity of the required hardware.

Frequency stabilization of lasers for atom-cooling and -trapping experiments is generally achieved via a feedback servo that controls the laser diode current and/or other feedback parameters. The signal used for this feedback is usually generated from spectroscopic measurements on an atomic vapor cell, although a range of other approaches is possible; see [16] for a full review of active laser frequency stabilization. A common technique with atomic vapor is based on saturated absorption spectroscopy [17,18], combined with modulation of the laser current and phase-sensitive detection of the spectroscopic signal [19].

Dual-frequency spectroscopy techniques were previously applied to stabilize lasers for multistep excitation processes [20] and the generation of Rydberg atoms [21], in atomic vapor magnetometry [22,23], and to address atypical atomic transitions [24]. Herein, we show the utility and unique benefits of the approach in the context of laser stabilization for cooling and trapping experiments; variation of both lasers' frequencies opens up a two-dimensional parameter space where optical pumping effects create a lattice of Doppler-free resonance features, offering an expanded set of potential "locking points" at which the lasers' frequencies can be stabilized. We show how two lasers can be stabilized simultaneously, with improved frequency stability, based on the resulting spectroscopic signals. This differs significantly from previous implementations in cooling and trapping experiments, which were based on fixed-frequency modulation of a single laser source [24–27].

*nathan.cooper@nottingham.ac.uk

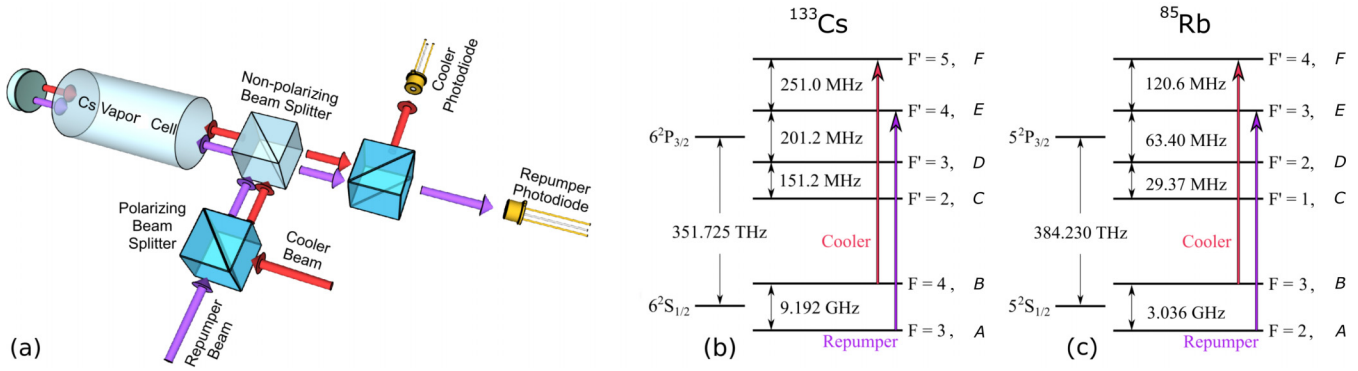

FIG. 1. (a) Experimental setup used for dual-beam spectroscopy. For clarity, the spatially overlapped laser beams are illustrated side by side. (b) Level structure for ^{133}Cs, indicating the role of the cooler and repumper lasers. (c) Level structure for ^{85}Rb.

These results are of particular relevance to the burgeoning field of portable quantum technologies [28–31]. Here, the achievable reductions in size, weight, and complexity offered by allowing multiple beams to share one spatial pathway are important. Furthermore, the drive for miniaturization increases the desirability of using small vapor cells with correspondingly reduced optical depths [32–35]. Operating these quantum technology systems outside the laboratory results in exposure to increased environmental noise, requiring improvements in signal strength and sensitivity. We analyze two examples for alkali atoms, ^{133}Cs and ^{85}Rb, which are frequently used and highly relevant in quantum technologies. The locking scheme was successfully applied in [30] to create a magneto-optical trap with 10^8 Rb atoms, without further description.

This paper is structured as follows: we describe the experimental implementation of this technique and present a rate-equation model that explains its key features. Experimental results spanning the full two-dimensional (2D) frequency space associated with dual-frequency spectroscopy are shown, and simultaneous frequency stabilization of lasers addressing two different transitions within the same atomic species is performed. As a result, the frequency stability of these lasers is found to be up to 3 times better than that achieved using conventional spectroscopic stabilization.

II. SETUP AND LAYOUT

Consider two orthogonally polarized laser beams from independent lasers, which are combined and spatially overlapped at a polarizing beam splitter. The two beams copropagate through a Doppler-free spectroscopy setup [18], sharing the same optical components, as illustrated in Fig. 1(a). After interacting with the cell the laser beams are separated at a polarizing beam splitter, and their intensities are individually recorded on separate photodiodes, yielding outputs V_1 and V_2. This configuration is chosen as required for most atomic physics experiments, which rely on two frequencies (cooler and repumper) for atom cooling, as shown for the examples of ^{133}Cs and ^{85}Rb in Fig. 1(b).

The frequencies of both beams are tuned close to resonance with the D_2 line of the relevant atomic species, in our case ^{133}Cs and ^{85}Rb: the repumper laser is resonant with transitions from the lower hyperfine state of the "ground" (S-state) manifold, and the cooler laser is resonant with transitions from the upper hyperfine state [see Fig. 1(b)]. Throughout this paper, laser frequencies will always be specified relative to the highest-frequency atomic transition in their respective manifolds, e.g., relative to the $F = 4 \rightarrow F' = 5$ transition for the cooler laser for ^{133}Cs.

The use of only a single optical frequency for spectroscopy on the D lines of alkali-metal atoms results in pumping of the atomic population into a state not addressed by the pumping light, just as observed in magneto-optical trapping experiments [15,36], leading to attenuation of the atomic response and a weaker spectroscopic signal. When light resonant with both cooler and repumper transitions is present [see Fig. 1(b)], there are no long-lived, noninteracting states in which atoms can accumulate; simultaneous use of both lasers therefore prevents attenuation of the spectroscopic signal via optical pumping. Figure 2 shows the results of this experiment with one laser frequency fixed and the other scanned, corresponding to a one-dimensional (1D) slice through the available parameter space, for ^{133}Cs. Figure 2(a) details the output of the repumper photodiode, with one laser scanned across the $F = 3 \rightarrow F' = 3, 4, 5$ transition (blue line), while light tuned to -365 MHz from the $F = 4 \rightarrow F' = 5$ transition is also present. The full experimental parameters used are given in Appendix B.

Figure 3 shows a comparable measurement for ^{85}Rb. Figure 3(a) presents the spectrum measured by the cooler photodiode, where one laser is scanned across the $F = 2 \rightarrow F' = 2, 3, 4$ transition, while light tuned to the $F = 3 \rightarrow F' = 3$ transition is also present (blue line). Figures 2(a) and 3(a) clearly show that the use of dual-frequency spectroscopy (blue line) substantially increases the overall absorption of the light by the atomic vapor and the size and spread of the sub-Doppler features in comparison to standard Doppler-free spectroscopy (gray line). The dashed lines represent a fit to the Doppler valley, i.e., the expected absorption in the absence of sub-Doppler features revealed by pump-probe spectroscopy; the spectroscopic signals are then locally normalized against this fit (a standard approach to removing the Doppler-broadened absorption and leaving only the desired sub-Doppler features) and differentiated with respect to the frequency of the scanned laser to yield the "error signal" S,

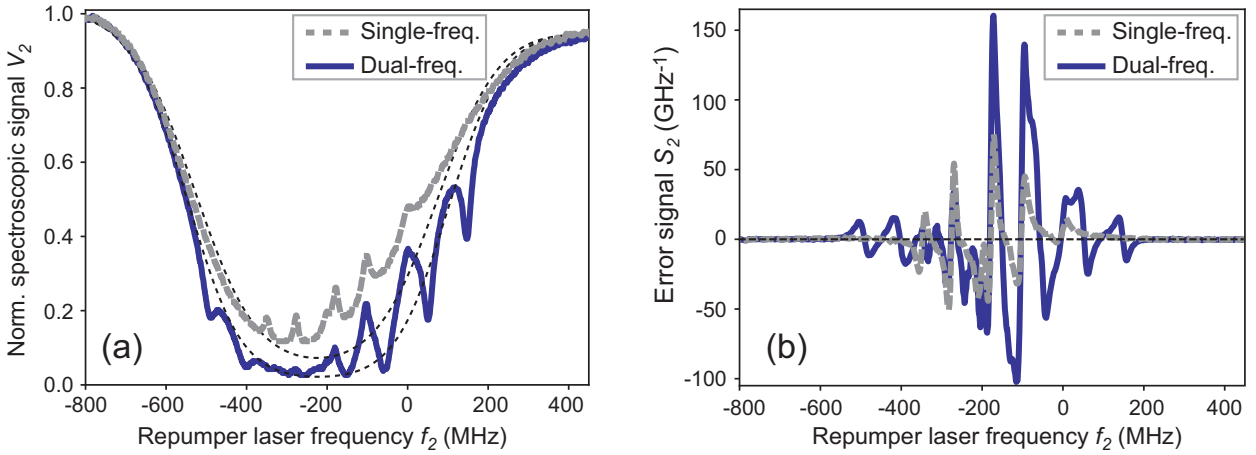

FIG. 2. (a): ^{133}Cs spectroscopy signal V_2 from the repumper photodiode [see Fig. 1(a)] while light from the cooler laser, tuned 365 MHz below the $F = 4 \rightarrow F' = 5$ transition, is also present in the cell (solid blue line). A standard Doppler-free saturated absorption spectroscopy signal (gray dashed line) is shown for reference, while the dotted lines are fits to the Doppler-broadened absorption profile in each case. The addition of light tuned to the cooler transition substantially increases the size and spread of the Doppler-free features. (b) Doppler-free error signal (see text) resulting from the spectroscopic signals in (a). In both panels, the laser-frequency axis is that of the repumper laser relative to the $F = 3 \rightarrow F' = 4$ transition.

plotted in Figs. 2(b) and 3(b); this is the signal typically used for feedback stabilization of a laser's frequency based on Doppler-free spectroscopy, and it is given by $S(f_i) = V_{\mathrm{DB},i}^{-1}(dV_i/df_i)$, where $V_{\mathrm{DB},i}$ is the photodiode signal corresponding to the fitted, Doppler-broadened light transmission for a given laser frequency, V_i denotes the measured photodiode output, and f_i is the frequency of the relevant laser.

The comparisons in Figs. 2(b) and 3(b) show how dual-frequency spectroscopy yields greater error signal sensitivity dS/df and broader capture ranges (the range of laser frequencies over which the sign of dS/df is unchanged) about the zero crossings of the error signal, known as the "lock points" because laser frequency can be stabilized most effectively at these values. In addition, a greater number of potential lock points become available over a wider frequency range than for conventional pump-probe spectroscopy.

III. MODEL AND THEORY

An intuitive analysis of this system can explain the enhanced absorption, the increased number of absorption peaks, and the latticelike structure observed in 2D frequency space, which is seen Figs. 4(a) and 5(a). When the cooler and repumper lasers are simultaneously resonant with atoms with similar velocities, the absorption of light from both beams is enhanced. For copropagating beams the simultaneous resonance condition requires that the two laser frequencies are separated by a fixed amount, thus creating a set of sharp

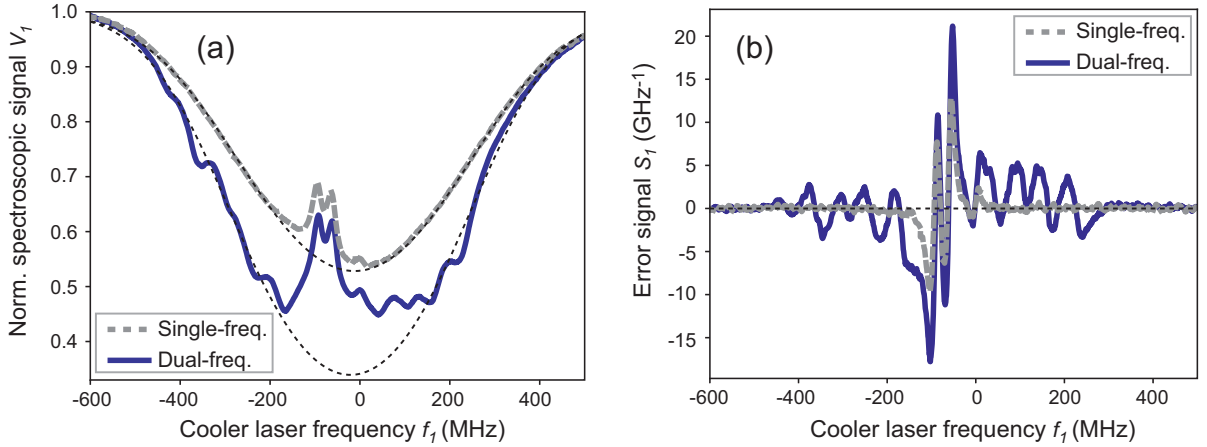

FIG. 3. (a) ^{85}Rb spectroscopy signal V_1 from the cooler photodiode [see Fig. 1(a)] while light from the repumper laser, resonant with the $F = 3 \rightarrow F' = 3$ transition, is also present in the cell (solid blue line). A standard Doppler-free saturated absorption spectroscopy signal (dashed gray line) is shown for reference, while the dotted lines are fits to the Doppler-broadened absorption profile in each case. The addition of light tuned to the repumper transition increases the size and spread of the Doppler-free features. (b) Doppler-free error signal (see text) resulting from the spectroscopic signals in (a). In both panels, the laser-frequency axis is that of the cooler laser relative to the $F = 4 \rightarrow F' = 5$ transition.

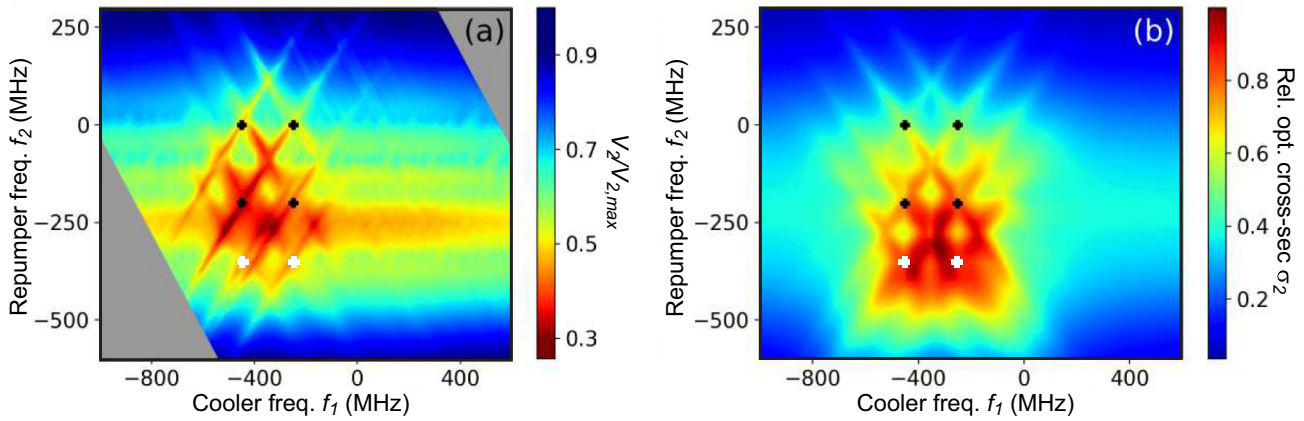

FIG. 4. (a) Spectroscopic signal V_2 from the ^{133}Cs repumper laser photodiode as a function of the frequencies of both lasers. Frequencies for the cooler and repumper lasers are given relative to the $F = 4 \rightarrow F' = 5$ and $F = 3 \rightarrow F' = 4$ transitions, respectively. (b) Prediction of the rate-equation model for the relative optical absorption cross section per atom from the repumper beam σ_2. To guide the eye, pluses indicate the points where the two lasers are simultaneously resonant with relevant transitions in stationary atoms such that optical pumping effects lead to diagonal line features; the black pluses represent transitions that produce line features in the absorption of both lasers, while the white pluses represent cycling transitions that do not heavily affect the absorption of the other laser. The rate-equation model describes the observed key features very well. The simulation assumes that the intensity of the return beam is always half of that of the incoming beam.

features, similar to those seen in saturated absorption spectroscopy, that map out diagonal lines of positive slope in 2D frequency space. For counterpropagating beams, the same effect is present, but the sign of the slope is reversed. Since both copropagating and counterpropagating beams are present in the vapor cell, the dual-frequency optical pumping effects can be expected to produce diagonal line features with both positive and negative slopes. We show below that the full lattice structure is required for efficient, simultaneous laser stabilization.

We develop a theoretical model that correctly predicts the key features of our results and elucidates the underlying physical mechanisms. For this the transient behavior of atoms traversing the beam is approximated as follows: we assume that some fraction of the atoms N_F recently entered the laser beam and remains in an equal mixture of the two hyperfine states of the $6S_{1/2}$ level. The remaining atomic population is taken to be in a state of dynamic equilibrium. This is a reasonable approximation, as very few cycles of optical pumping are required to redistribute the atomic population.

To determine the influence of these "equilibrium-state" atoms on the spectroscopic signals, we adopt a similar approach to [37], developing a rate-equation-based model in which we consider the six-level systems shown in Fig. 1. For convenience, we label the atomic states A–F, in ascending order from the bottom of the figure. For now, consider only a single atom with fixed laser detunings—the thermal distribution of atomic velocities and corresponding Doppler shifts will be factored in later. We define a set of rate coefficients, τ_{ij} and Γ_{ij}, such that the stimulated and spontaneous transition rates between, for example, states E and B are given by $\tau_{EB}I_{EB}$ and Γ_{EB}, respectively, where I_{EB} is the intensity of the laser light tuned to the relevant set of transitions (i.e., cooler or repumper). The spontaneous decay rates for the

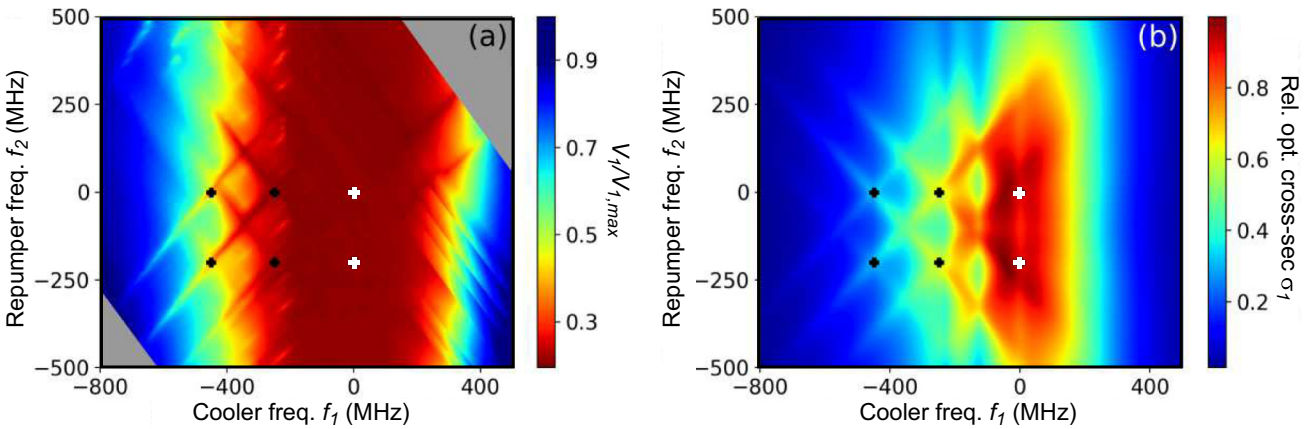

FIG. 5. (a) Spectroscopic signal V_1 from the ^{133}Cs cooler laser photodiode as a function of the frequencies of both lasers. (b) Corresponding theoretical prediction for the optical absorption cross section per atom σ_1. Both panels are analogous to their counterparts in Fig. 4 and were produced under the same conditions.

relevant transitions are already known accurately; see, for example, [38]. To determine the rate coefficients for stimulated transitions, we equate the steady-state results for the upper state population produced by our rate-equation model to those produced by solving the full optical Bloch equations for a two-level system. For a transition with spontaneous decay rate Γ, illumination of detuning δ, and intensity I, with Rabi frequency Ω, we obtain

$$\frac{\Omega^2/4}{\delta^2+\Omega^2/2+\Gamma^2/4}=\frac{\tau I}{2\tau I+\Gamma}. \tag{1}$$

Therefore, labeling the dipole matrix element $\langle E|x|B\rangle$ between two levels as X_{EB}, we find that

$$\tau_{EB}=\frac{\Omega_{EB}^2\Gamma_{EB}}{4I_{EB}\left(\delta_{EB}^2+\Gamma_{EB}^2/2\right)}=\frac{e^2|X_{EB}|^2\Gamma_{EB}}{2\hbar^2c\epsilon_0\left(\delta_{EB}^2+\Gamma_{EB}^2/2\right)}, \tag{2}$$

with similar results for the other transitions. Hence, using each state's label to denote the population fraction in that state, the rate equations governing the system are given by

$$\frac{dF}{dt}=(B-F)\tau_{FB}I_{FB}-F\Gamma_{FB}, \tag{3}$$

with corresponding expressions for the time derivatives of the populations of the remaining states (see Appendix A). Setting all time derivatives to zero and the total population across all states equal to 1, we solve the equations to find the fractional steady-state populations in each state. The full derivation is given in Appendix A. Here, we simply quote the result, first defining the following notation:

$$\gamma_{ij}=\tau_{ij}I_{ij}+\Gamma_{ij}, \tag{4}$$

$$k_{ij}=\frac{\tau_{ij}I_{ij}}{\sum_k\gamma_{ik}}, \tag{5}$$

$$\zeta_i=\frac{1}{\sum_j\tau_{ji}I_{ji}}, \tag{6}$$

and the composite coefficient

$$\Phi=\frac{(k_{EA}\gamma_{EB}+k_{DA}\gamma_{DB})\zeta_B}{1-(k_{FB}\gamma_{FB}+k_{EB}\gamma_{EB}+k_{DB}\gamma_{DB})\zeta_B}, \tag{7}$$

with summations carried out only where explicitly indicated, over all dipole-allowed transitions. We find that in the steady state

$$A=\left[1+\sum_i k_{iA}+\Phi\left(1+\sum_j k_{jB}\right)\right]^{-1}, \tag{8}$$

with the remaining fractional populations given by

$$B=\Phi A, \tag{9}$$

and for the upper manifold

$$i=k_{iA}A+k_{iB}B, \tag{10}$$

where $i\in\{C,D,E,F\}$, as given in Fig. 1.

Having obtained the steady-state populations, we can now determine the rate of photon loss per equilibrium-state atom $L_{\rm eq}$ from a given beam as

$$L_{\rm eq}=\sum(j-i)\tau_{ij}I_{ij}, \tag{11}$$

where the sum is taken over all combinations of upper manifold states i and lower manifold states j between which dipole-allowed transitions can be stimulated by the chosen beam ignoring the negligible stimulation of cooler (repumper) transitions by repumper (cooler) lasers. The unpumped atoms can be taken into consideration at this stage as well, yielding

$$L=(1-N_F)\sum(j-i)\tau_{ij}I_{ij}+N_F\sum\frac{1}{2}\tau_{ij}I_{ij}. \tag{12}$$

Equation (12) can be used to determine the rate of attenuation of a laser beam by stationary atoms subject to known illumination conditions. To accurately model a thermal atomic vapor, the velocity distribution of the atoms and corresponding Doppler shift in each beam's effective detuning must be taken into account. This can be done by integrating Eq. (12) over the atomic velocity distribution, where the dependence of L on atomic velocity comes in via the dependence of the values of δ_{ij} in Eq. (2) on atomic velocity (due to the Doppler shift) and the corresponding variation in the values of τ_{ij}. We define $L_{\rm thermal}$ as the average loss rate of photons from the beam per atom, given the atoms' thermal velocity distribution. In the case of a thermal atomic vapor at temperature T, considering only the first-order Doppler shift, this is given by

$$L_{\rm thermal}=\frac{1}{N}\int_{-\infty}^{\infty}L(v)\exp\left(-mv^2/2k_{\rm B}T\right)dv, \tag{13}$$

where m is the mass of the atoms, $k_{\rm B}$ is the Boltzmann constant, and the integration variable v corresponds to the atomic velocity component along the axis of the laser beams. $N=\sqrt{2\pi k_{\rm B}T/m}$ is the normalization constant for the 1D Boltzmann distribution. Furthermore, one must consider that there are counterpropagating beams within the vapor cell. These can be taken into account by summing the contributions of the different beams to the stimulated transition rates, such that in the equations above $\tau_{ij}I_{ij}$ becomes $\tau_{ij}I_{ij}(\text{beam 1})+\tau_{ij}I_{ij}(\text{beam 2})$. Note that for counterpropagating beams the signs of the Doppler shift on the value of δ_{ij} in Eq. (2) will be opposite for the two beams.

With this substitution made, Eq. (13) can be used to deduce the mean optical absorption cross section per atom [39]. for a given laser as a function of both laser frequencies; normalized against its maximum value, we label the absorption cross section per atom σ_1 and σ_2 for the repumper and cooler lasers, respectively.

The results are shown in Figs. 4 and 5 alongside our experimental data. The theoretical model explains the key observed features well. The presence of each beam increases the strength of the absorption of the other beam and creates sharp locking features, similar to those seen in saturated absorption spectroscopy, in a diagonal crisscross pattern across the Doppler valley. Exact, quantitative agreement requires a more complex model that is not developed here.

IV. EXPERIMENTAL RESULTS

Figures 4 and 5 show the output signals from the photodiodes depicted in Fig. 1(a) as a function of the frequencies of both the cooler and repumper lasers for the case of ^{133}Cs. These were obtained by synchronously scanning both laser frequencies across the relevant frequency range. This results

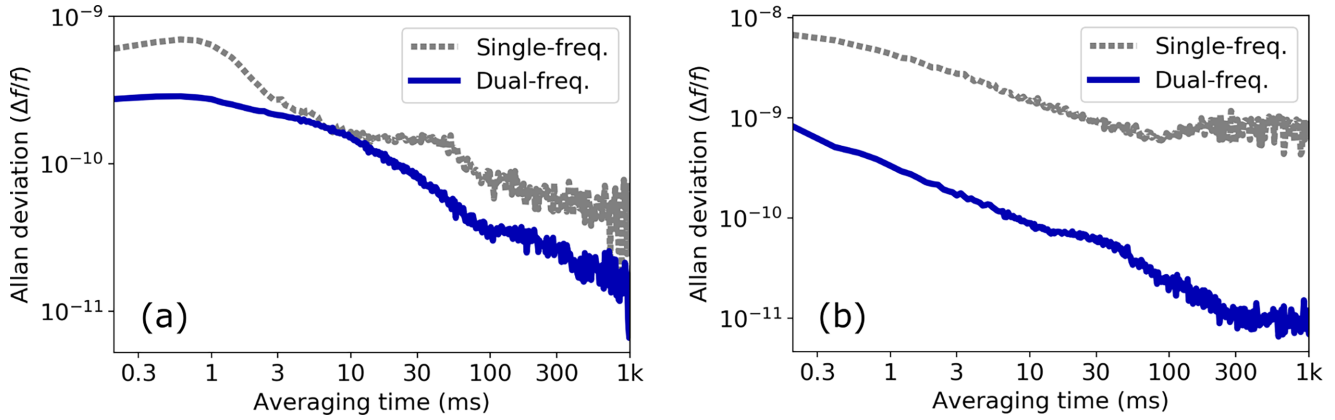

FIG. 6. Measured Allan deviation of the frequency of lasers stabilized to the (a) cooler and (b) repumper transitions of the D_2 line of ^{85}Rb, using both dual-frequency (solid blue line) and conventional Doppler-free (dotted gray line) spectroscopy to generate the feedback signal for laser stabilization. Note that the point of interest is not the absolute degree of stability achieved, but the improvement consistently provided by employing the dual-frequency spectroscopy scheme.

in the collection of data along diagonal lines in 2D frequency space. The gray area in Figs. 4 and 5 indicates parts between the plot axes where no data have been taken.

Figure 4(a) shows the output of the repumper photodiode V_2 for ^{133}Cs in comparison to the result of the rate-equation model in Fig. 4(b). An independent frequency reference was provided by simultaneously directing light from each of the lasers to a standard saturated absorption spectroscopy apparatus. The rate-equation model reproduces the experimentally observed features well for a 75-mm cell at 298 K. The diameter of each beam was 1.25 mm, with 0.14 mW of cooler light and 0.23 mW of repumper light present.

Figures 4 and 5 show that the rate-equation model successfully explains the key features of the technique and predicts qualitative trends; the numerical model reveals both the enhanced absorption and the existence and origins of the diagonal line features observed. A quantitative comparison is not attempted due to the simplifications involved in the model. The core benefits of dual-frequency spectroscopy are clearly visible in both spectra: the presence of the additional cooler (repumper) frequency light enhances the absorption signal of the repumper (cooler) light by the atomic vapor and generates sharp, sub-Doppler features in a diagonal grid pattern over a frequency range of about 700 MHz—considerably broader than the 450 MHz (for the cooler laser) or 350 MHz (for the repumper laser) over which conventional saturated absorption spectroscopy produces Doppler-free resonance features. This enables the technique to be used for frequency stabilization at a wider range of frequency offsets than is usually possible.

The enhancement of the absorption signal is also shown in Fig. 2(a). For reference, the blue dual-frequency data displayed in Fig. 2(a) would correspond to a vertical slice through Fig. 4(a) at a cooler frequency of −365 MHz, while the conventional, single-frequency spectrum [gray data in Fig. 2(a)] would be reproduced by a vertical slice in the limit of large detuning of the cooler laser. The strong observed enhancement of the absorption signal translates to more accurate laser frequency stabilization by providing a feedback signal with improved sensitivity and signal-to-noise ratio. This will be discussed and characterized in the next section.

V. APPLICATION TO LASER FREQUENCY STABILIZATION

As shown above, dual-frequency spectroscopy offers improved feedback signal strength and sensitivity compared to conventional spectroscopy. The dual-frequency error signals allow superior laser frequency stabilization for two lasers simultaneously, as seen in Fig. 6, which is discussed in more detail below.

The simplest way to achieve this is to select the correct locations in 2D frequency space (lock points) at which to stabilize the lasers' frequencies; in general, the dual-frequency stabilization signal for each laser can depend on the frequency of the other laser, but efficient frequency stabilization is possible at lock points where the local gradient of each laser's stabilization signal with respect to the other laser's frequency is zero or at a wider range of points through the use of a composite feedback signal (see Appendix C).

The simplest approach to this, and the one we adopt in our cold-atom experiment [30,31], is to stabilize the lasers at positions in 2D frequency space where, to first order in frequency changes about the chosen point, there is no dependence of the error signal for one laser on the frequency of the other laser, i.e.,

$$\frac{dS_1}{df_2} = \frac{d^2V_1}{df_1 df_2} = 0, \tag{14}$$

with the corresponding condition for dS_2/df_1. Figure 7 shows the "cross derivatives"—the derivatives of the absorption strength for one laser with respect to both laser frequencies—for ^{133}Cs as an example. These are derived as $d^2\sigma_1/(df_1 df_2)$ and $d^2\sigma_2/(df_2 df_1)$ from the results shown in Figs. 5(b) and 4(b).

From Fig. 7, one can identify the positions where these derivatives are both zero and, therefore, independent laser frequency stabilization (to first order) is possible. The corresponding figure for Rb is given in Appendix D. In particular, this condition is fulfilled wherever local maxima or minima in both V_1 and V_2 are coincident in frequency space. A local minimum in both signal voltages occurs at each of the intersections of the lines of positive and negative slope in 2D frequency

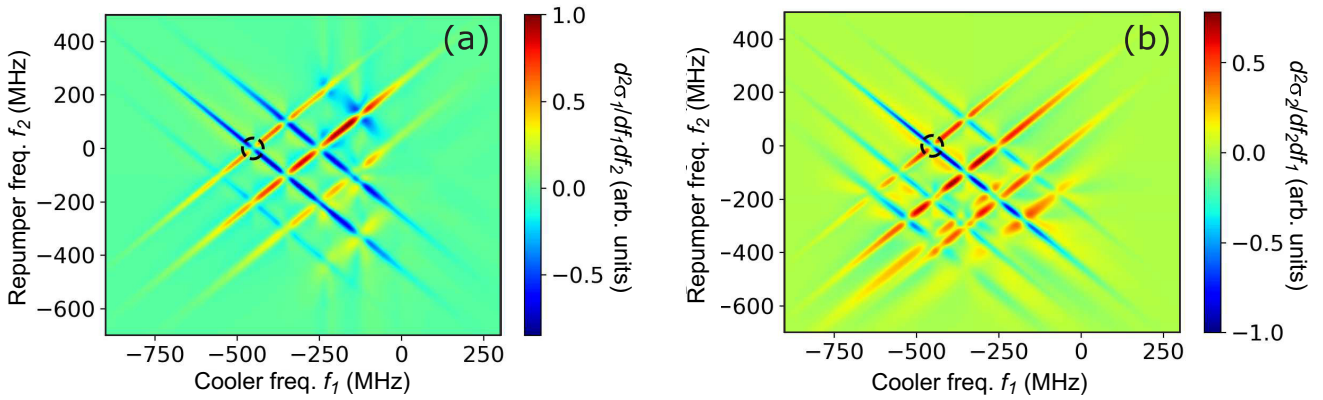

FIG. 7. Normalized cross derivatives (see text) of the theoretical optical absorption cross section per atom σ for ^{133}Cs (a) cooler and (b) repumper lasers, with respect to the frequencies of both lasers, $d^2\sigma_1/(df_1df_2)$ and $d^2\sigma_2/(df_2df_1)$, respectively. Zeros of these derivatives, such as those that occur at the intersections of the diagonal line features of opposite slope, are locations where the lasers can be simultaneously stabilized without interdependence of their lock points. The dashed black circles highlight one such point, showing that the zero of the cross derivative occurs at the same point in frequency space for both lasers.

space that occur in both laser signals; see, for example, the point highlighted in Fig. 7. This immediately creates a number of suitable locking points equal to the square of the number of relevant transition pairings (corresponding to the four black diamonds that are common to both Figs. 4 and 5). The locations of these locking points depend only on the frequency of the two lasers, not on the applied optical power (except for extremely high or low illumination intensities that would not be used in real experiments); the method is therefore not adversely affected by changes in incident optical power. As an example, for ^{133}Cs this yields 16 potential dual-frequency locking points, well in excess of the ∼5 plausible locking points generally usable with conventional spectroscopic stabilization. Furthermore, these lock points are spread over a frequency range 200 MHz broader than the standard transition manifold, allowing more flexibility for off-resonant laser stabilization.

The stability of two simultaneously locked lasers is characterized in Fig. 6 by determining the Allan deviation of the laser frequencies for averaging times between 0.2 ms and 1 s and compared to conventional Doppler-free spectroscopic stabilization with otherwise identical system parameters. The frequency stability was measured by logging the deviation of the stabilization signal from zero over a period of 10 s. Figure 6 compares dual-frequency stabilization to the $F = 3 \rightarrow F' = 3$ and $F = 2 \rightarrow F' = 3$ transitions of ^{85}Rb against individual stabilization to the $F = 3 \rightarrow F' = 4$ transition and the $F = 2 \rightarrow F' = 2 \otimes 3$ crossover transition [40].

The absolute values of the frequency stability achieved are within the expected range, being superior to those measured in systems with a broader response, such as wavemeter-based stabilization [41] but inferior to those obtained with custom-built, ultrastable laser systems [42,43]. Since our cooler and repumper lasers employ very different hardware—a butterfly packaged-distributed-feedback laser and an external cavity diode laser, respectively—they experience different technical sources of frequency instability, so the differing time profiles of their Allan deviations are not unexpected.

The improvement in stability achieved through the use of dual-frequency spectroscopy, within an otherwise identical system, is clearly visible in Fig. 6 and, for the cooler laser, corresponds approximately to the improvement expected from the increase in the gradient of the stabilization feedback signal over most of the range of averaging times studied. Over a small range of averaging times on the order of 10 ms the Allan deviation for the cooler laser becomes comparable using both single- and dual-frequency spectroscopy; the reason for this are not fully understood, but it may be related to nontrivial coupled feedback effects in the laser stabilization electronics and is likely a technical artifact specific to our experimental arrangement.

Similarly, the full stability improvement seen for the repumper laser—a factor >10 over most of the range of averaging times studied—cannot be explained by our model. The better than expected performance here could stem from technical considerations specific to our feedback hardware or from a sharpening of the atomic response by coherent effects omitted from our rate-equation model.

Going beyond the method described here, a broader range of locking points can be accessed through the generation of composite feedback signals that are a function of the outputs from both photodiodes; this technique is explained in detail in Appendix C.

For simultaneous laser stabilization using dual-frequency spectroscopy, both lasers must be brought to and maintained at frequencies close to the desired locking point while the feedback control is engaged. If passive laser stability is poor, this can be slightly more challenging than locking a single laser. This difficulty can be mitigated with customized control electronics and user interfaces.

VI. CONCLUSIONS

Our results show that the use of spatially overlapping beams tuned to different atomic transitions can allow optical pumping effects to be exploited to enhance signal strength in atomic vapor spectroscopy. Optical pumping effects lead to a large number of crossover features, allowing laser stabiliza-

tion at a greater range of frequencies than via conventional Doppler-free spectroscopy. The technique provides clear advantages wherever two frequencies are required and space, weight, and optical components are at a premium, as well as in situations where signal strength and frequency sensitivity are important. This applies to a number of quantum technology research areas, ranging from portable devices such as gravimeters, magnetometers, and atomic clocks to precision laboratory-based experiments where the accuracy of laser frequency stabilization is paramount.

We provided detailed data on spectroscopy on the D_2 lines of cesium and rubidium in unheated, 75-mm-long cells at 20 °C. The enhanced contrast of the absorption signal is particularly relevant for short vapor cells [34,35,44]. The same principles demonstrated here will apply within any atomic vapor that exhibits sharp, saturable optical transitions. In particular, the absence of a "cycling transition" in lower-mass alkali-metal atoms (Li, Na, and K), brought about by the small energy separation of the hyperfine states of the upper manifold of the D_2 lines, suggests that the benefits of avoiding optical pumping to dark states may be enhanced for these species.

Future extensions of this technique include demodulation of the signal from one photodiode at the current modulation frequencies of both lasers, thus yielding two different derivative signals from each photodiode (e.g., dV_1/df_1 and dV_1/df_2 from the cooler photodiode) and enabling frequency stabilization at almost any point in 2D frequency space. Dual-frequency forms of modulation transfer spectroscopy [45] should also be possible, allowing this important technique to be exploited through current modulation of either one of the two lasers, avoiding the need for costly electro-optic modulation equipment. Finally, including further laser frequencies may open up yet more technical possibilities and reveal additional physical phenomena.

All data necessary to support the conclusions of this paper are given in the paper. All further data related to this work are available from the authors upon request.

ACKNOWLEDGMENTS

The authors thank B. Foxon and I. Lesanovsky for useful discussions and R. Chacko for assistance with data collection. This work was supported by IUK Projects No. 133086 and No. 10031462, EPSRC Grants No. EP/R024111/1 and No. EP/M013294/1, JTF Grant No. 62420, and the European Commission grant ErBeStA (Grant No. 800942).

The authors declare the following competing interests: N.C. and L.H. are inventors on UK pending patent application GB 1916446.6 (applicant: University of Nottingham, inventors: Nathan Cooper, Lucia Hackermüller, Laurence Coles) for a miniaturized spectroscopy device in which dual-frequency beam overlap is exploited as an aid to compactness.

APPENDIX A: RATE EQUATION MODEL

We provide the expressions for the time derivatives of the remaining atomic state populations:

$$\frac{dE}{dt} = (A-E)\tau_{EA}I_{EA} + (B-E)\tau_{EB}I_{EB} - E\Gamma_{EB} - E\Gamma_{EA}, \tag{A1}$$

$$\frac{dD}{dt} = (B-D)\tau_{DB}I_{DB} + (A-D)\tau_{DA}I_{DA} - D\Gamma_{DB} - D\Gamma_{DA}, \tag{A2}$$

$$\frac{dC}{dt} = (A-C)\tau_{CA}I_{CA} - C\Gamma_{CA}, \tag{A3}$$

$$\frac{dB}{dt} = (F-B)\tau_{FB}I_{FB} + (E-B)\tau_{EB}I_{EB} + (D-B)\tau_{DB}I_{DB} + F\Gamma_{FB} + E\Gamma_{EB} + D\Gamma_{DB}, \tag{A4}$$

and

$$\frac{dA}{dt} = (E-A)\tau_{EA}I_{EA} + (D-A)\tau_{DA}I_{DA} + (C-A)\tau_{CA}I_{CA} + E\Gamma_{EA} + D\Gamma_{DA} + C\Gamma_{CA}. \tag{A5}$$

Then, employing the terms defined in Eq. (1), (2), and (4)–(7) and setting all time derivatives to zero, as is the case in the steady state, Eq. (3) and its counterparts above can be rearranged to give

$$F = \frac{B\tau_{FB}I_{FB}}{\gamma_{FB}} = Bk_{FB}, \tag{A6}$$

$$E = \frac{A\tau_{EA}I_{EA} + B\tau_{EB}I_{EB}}{\gamma_{EA}+\gamma_{EB}} = Ak_{EA} + Bk_{EB}, \tag{A7}$$

$$D = \frac{A\tau_{DA}I_{DA} + B\tau_{DB}I_{DB}}{\gamma_{DA}+\gamma_{DB}} = Ak_{DA} + Bk_{DB}, \tag{A8}$$

$$C = \frac{A\tau_{CA}I_{CA}}{\gamma_{CA}} = Bk_{CA}, \tag{A9}$$

$$B = \frac{D\gamma_{DB} + E\gamma_{EB} + F\gamma_{FB}}{\tau_{DB}I_{DB} + \tau_{EB}I_{EB} + \tau_{FB}I_{FB}} = \frac{D\gamma_{DB} + E\gamma_{EB} + F\gamma_{FB}}{\zeta_B}, \tag{A10}$$

and

$$A = \frac{C\gamma_{CA} + D\gamma_{DA} + E\gamma_{EA}}{\tau_{CA}I_{CA} + \tau_{DA}I_{DA} + \tau_{EA}I_{EA}} = \frac{C\gamma_{CA} + D\gamma_{DA} + E\gamma_{EA}}{\zeta_A}. \tag{A11}$$

Substitution of Eqs. (A6) to (A8) into (A10) then yields

$$B = \zeta_B^{-1}[\gamma_{DB}(Ak_{DA} + Bk_{DB}) + \gamma_{EB}(Ak_{EA} + Bk_{EB}) + \gamma_{FB}Bk_{FB}]. \tag{A12}$$

Collecting terms in A and B and dividing through by the coefficient of B, one finds that

$$B = \Phi A. \tag{A13}$$

Now all other state populations can be expressed in terms of A. As a final constraint, we impose the condition that the sum over all state-population fractions must be equal to 1. Expressing all state populations in terms of A and setting their sum equal to 1 yields Eq. (8). Combining this with Eq. (A6) to (A9) and (A13) above directly gives all of the steady-state population fractions.

APPENDIX B: DETAILS OF EXPERIMENTAL DATA COLLECTION

During the data collection for Fig. 2 in the main text, 0.37 mW of cooler light, at a fixed frequency of −365 MHz (relative to the $F = 4 \rightarrow F' = 5$ transition), was directed into the apparatus alongside 0.25 mW of repumper light. For Fig. 3, the same beam diameters were used with 0.17 mW of cooler light and 0.42 mW of repumper light. The repumper light was resonant with the $F = 3 \rightarrow F' = 3$ transition of the D_2 line of ^{85}Rb.

In Figs. 4(a) and 5(a) optical transmission data were collected across a broad region of 2D frequency space by synchronously scanning the frequencies of both lasers. Synchronous laser frequency ramps were performed by adding a linear ramp to the current supplied to each laser diode and simultaneously ramping the voltage supplied to piezoelectric transducers that control the alignment of diffraction gratings used for external cavity feedback. The result is laser frequencies, f_1 and f_2, described by

$$f_1 = a + bt, \quad f_2 = c + dt, \tag{B1}$$

where t is the time since the start of the ramp, f_1 and f_2 are the frequencies of the cooler and repumper lasers, respectively, and a–d are constant coefficients. The resulting equation expressing f_2 as a function of f_1 is

$$f_2 = \frac{d}{b} f_1 + \left(c - \frac{da}{b}\right). \tag{B2}$$

This equation describes a diagonal line in the parameter plane displayed in Fig. 4, with gradient d/b and offset $c - (da/b)$. By adjusting either of the static frequency offsets, a and c, data along multiple such lines were collected and used to build up a full 2D data set as displayed. Note that the boundaries of the region within which data were collected consequently form diagonal lines in 2D frequency space, hence the grayed-out triangles in the corners of Figs. 4(a) and 5(a). The spectroscopic signals from conventional, single-frequency spectroscopy apparatus were collected at the same time for each laser, enabling independent determination of laser frequency.

APPENDIX C: STABILIZATION WITH NONZERO CROSS DERIVATIVES

In the main text laser frequency stabilization at selected locations in 2D frequency space was considered, where the derivative of each laser's stabilization signal with respect to the frequency of the other laser was zero. However, a more general method exists that enables frequency stabilization at a much wider range of locations within 2D frequency space. Consider two lasers with frequencies f_1 and f_2 generating corresponding photodiode outputs V_1 and V_2. We assume that the currents of the two lasers are modulated at different frequencies to avoid direct cross talk.

Evaluating all derivatives at the chosen locking point, the gradient of the spectroscopic signal after demodulation S_1 is given by

$$\frac{dS_1}{df_1} = \vartheta_1 \frac{d^2V_1}{df_1^2} \tag{C1}$$

and

$$\frac{dS_1}{df_2} = \vartheta_1 \frac{d^2V_1}{df_1\, df_2}, \tag{C2}$$

where ϑ_1 and ϑ_2 are constants that depend on the parameters of the laser current modulation, with corresponding expressions for the gradient of S_2. One can therefore define a composite parameter χ_1 with no first-order dependence on f_2:

$$\chi_1 = S_1 - \kappa_1 S_2, \tag{C3}$$

where

$$\kappa_1 = \frac{\vartheta_1}{\vartheta_2} \frac{d^2V_1}{df_1\, df_2} \left(\frac{d^2V_2}{df_2^2}\right)^{-1}, \tag{C4}$$

with the value of κ_1 being determined by the requirement that the contributions of the first and second terms in (C3) to the gradient of χ_1 with respect to f_2 cancel. Corresponding expressions exist for χ_2. Thus, it is possible to generate a feedback signal for each laser that is, to first order, independent of the frequency of the other laser.

To determine the expected laser frequency stability when using this approach, one can define the "signal-limited stability factor" (M_{SL}), which is equal to the ratio of the sensitivity of the spectroscopic signal (to changes in laser frequency, about the desired lock point) in dual-frequency spectroscopy to the same parameter in a conventional spectroscopic setup; in this case the SLSF for laser 1 is therefore given by

$$M_{\mathrm{SL},1} = \frac{d\chi_1}{df_1} \Bigg/ \left(\frac{dS_{\mathrm{con}}}{df_{\mathrm{con}}} \sqrt{1 + \kappa_1^2}\right), \tag{C5}$$

where $dS_{\mathrm{con}}/df_{\mathrm{con}}$ is the gradient of the feedback signal about the lock point in an equivalent conventional saturated absorption spectroscopy apparatus. The factor of $\sqrt{1 + \kappa_1^2}$ normalizes against the amplification of the feedback signal that has been performed via postprocessing. One therefore finds that

$$M_{\mathrm{SL},1} = \left(\frac{dS_1}{df_1} - \kappa_1 \frac{dS_2}{df_1}\right) \Bigg/ \left(\frac{dS_{\mathrm{con}}}{df_{\mathrm{con}}} \sqrt{1 + \kappa_1^2}\right), \tag{C6}$$

with an equivalent expression for $M_{\mathrm{SL},2}$. This factor represents the quality of the frequency stabilization that can be achieved at any given locking point; lasers can be stabilized with superior performance to conventional spectroscopy at any location where both SLSF values exceed 1.

APPENDIX D: CROSS DERIVATIVES AND LOCKING POINTS FOR ^{85}Rb

By applying our theoretical model to ^{85}Rb, we obtain the structure of the cross derivatives of the optical

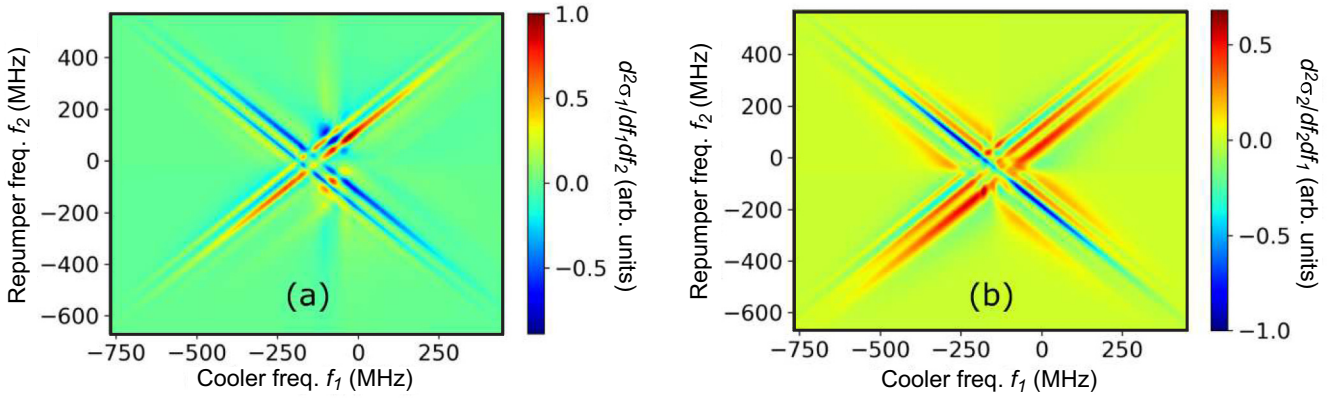

FIG. 8. Normalized cross derivatives of the theoretical optical absorption cross section per atom σ for ^{85}Rb (a) cooler and (b) repumper lasers, analogous to those shown in Fig. 7 for ^{133}Cs, with respect to the frequencies of both lasers. Zeros of this derivative, such as those that occur at the intersections of the diagonal line features of opposite slope, are locations where the lasers can be simultaneously stabilized without interdependence of their lock points.

absorption cross section for this species. Figure 8 shows the cross derivatives $d^2\sigma_1/(df_1df_2)$ and $d^2\sigma_2/(df_2df_1)$ vs f_1 and f_2 and highlights suitable locking points for the case of ^{85}Rb.

[1] I. Georgescu, 25 years of BEC, Nat. Rev. Phys. **2**, 396 (2020).

[2] J. Kitching, S. Knappe, and E. Donley, Atomic sensors—A review, IEEE Sens. J. **11**, 9 (2011).

[3] K. Van Tilburg, N. Leefer, L. Bougas, and D. Budker, Search for Ultralight Scalar Dark Matter with Atomic Spectroscopy, Phys. Rev. Lett. **115**, 011802 (2015).

[4] F. Sorrentino, K. Bongs, P. Bouyer, L. Cacciapuoti, M. De Angelis, H. Dittus, W. Ertmer, A. Giorgini, J. Hartwig, M. Hauth *et al.*, A compact atom interferometer for future space missions, Microgravity Sci. Technol. **22**, 551 (2010).

[5] S. Herrmann, H. Dittus, and C. Lammerzahl, Testing the equivalence principle with atomic interferometry, Classical Quantum Gravity **29**, 184003 (2012).

[6] P. Graham, J. Hogan, M. Kasevich, S. Rajendran, and R. Romani, Mid-band gravitational wave detection with precision atomic sensors, arXiv:1711.02225.

[7] I. Alonso, C. Alpigiani, B. Altschul, H. Araujo, G. Arduini, J. Arlt, L. Badurina, A. Balaz, S. Bandarupally, B. Barish, M. Barone, M. Barsanti, and S. Bass, Cold atoms in space: Community workshop summary and proposed road-map, EPJ Quantum Technol. **9**, 30 (2022).

[8] L. Badurina, E. Bentine, D. Blas, K. Bongs, D. Bortoletto, T. Bowcock, K. Bridges, W. Bowden, O. Buchmueller, C. Burrage *et al.*, AION: An atom interferometer observatory and network, J. Cosmol. Astropart. Phys. 05 (2020) 011.

[9] S. Bize, P. Laurent, M. Abgrall, H. Marion, I. Maksimovic, L. Cacciapuoti, J. Grünert, C. Vian, F. Pereira dos Santos, P. Rosenbusch, P. Lemonde, G. Santarelli, P. Wolf, A. Clairon, A. Luiten, M. Tobar, and C. Salomon, Cold atom clocks and applications, J. Phys. B **38**, S449 (2005).

[10] Y. Bidel, O. Carraz, R. Charriere, M. Cadoret, N. Zahzam, and A. Bresson, Compact cold atom gravimeter for field applications, Appl. Phys. Lett. **102**, 144107 (2013).

[11] V. Menoret, P. Vermeulen, N. Le Moigne, S. Bonvalot, P. Bouyer, A. Landragin, and B. Desruelle, Gravity measurements below 10^{-9} g with a transportable absolute quantum gravimeter, Sci. Rep. **8**, 12300 (2018).

[12] A. Fregosi, C. Gabbanini, S. Gozzini, L. Lenci, C. Marinelli, and A. Fioretti, Magnetic induction imaging with a cold-atom radio frequency magnetometer, Appl. Phys. Lett. **117**, 144102 (2020).

[13] E. Boto, N. Holmes, J. Legget, G. Roberts, V. Shah, S. S. Meyer, L. Duque Muñoz, K. J. Mullinger, T. M. Tierney, S. Bestmann, G. R. Barnes, R. Bowtell, and M. J. Brookes, Moving magnetoencephalography towards real-world applications with a wearable system, Nature (London) **555**, 657 (2018).

[14] C. Deans, L. Marmugi, and F. Renzoni, Sub-Sm^{-1} electromagnetic induction imaging with an unshielded atomic magnetometer, Appl. Phys. Lett. **116**, 133501 (2020).

[15] E. L. Raab, M. Prentiss, A. Cable, S. Chu, and D. E. Pritchard, Trapping of Neutral Sodium Atoms with Radiation Pressure, Phys. Rev. Lett. **59**, 2631 (1987).

[16] Y. Wu, B. Sun, and X. Li, Semiconductor laser active frequency stabilization technologies: A review, J. Korean Phys. Soc. **79**, 795 (2021).

[17] D. W. Preston, Doppler-free saturated absorption: Laser spectroscopy, Am. J. Phys. **64**, 1432 (1996).

[18] W. Demtröder, *Laser Spectroscopy* (Springer, Berlin, 2008).

[19] F. Riehle, *Frequency Standards: Basics and Applications* (Wiley-VCH, Weinheim, 2006).

[20] P. Mandal, V. Naik, V. Dev, A. Chakrabarti, and A. Ray, Blue fluorescence as a frequency offset reference in the rubidium 5S-5P-5D transition, Appl. Opt. **57**, 3612 (2018).

[21] D. Fahey and M. Noel, Excitation of Rydberg states in rubidium with near infrared diode lasers, Opt. Express **19**, 17002 (2011).

[22] V. Schultze, T. Scholtes, R. Ijsselsteijn, and H. Meyer, Improving the sensitivity of optically pumped magnetometers by hyperfine repumping, J. Opt. Soc. Am. B **32**, 730 (2015).

[23] R. Li, C. Perrella, and A. Luiten, Repumping atomic media for an enhanced sensitivity atomic magnetometer, Opt. Express **30**, 31752 (2022).

[24] M. Zhao, X. Jiang, R. Fang, Y. Qiu, Z. Ma, C. Han, B. Lu, and C. Lee, Laser frequency stabilization via bichromatic Doppler-free spectroscopy of an ^{87}Rb D_1 line, Appl. Opt. **60**, 5203 (2021).

[25] M. Hafiz, G. Coget, E. Clercq, and R. Boudot, Doppler-free spectroscopy on the Cs D1 line with a dual-frequency laser, Opt. Lett. **41**, 2982 (2016).

[26] M. Abdel Hafiz, D. Brazhnikov, G. Coget, A. Taichenachev, V. Yudin, E. Clercq, and R. Boudot, High-contrast sub-Doppler absorption spikes in a hot atomic vapor cell exposed to a dual-frequency laser field, New J. Phys. **19**, 073028 (2017).

[27] D. Brazhnikov, S. Ignatovic, I. Mesenzova, A. Mikhailov, R. Boudot, and M. Skortsov, Two-frequency sub-Doppler spectroscopy of the caesium D1 line in various configurations of counterpropagating laser beams, Quantum Electron. **50**, 1015 (2020).

[28] P. Knight and I. Walmsley, UK national quantum technology programme, Quantum Sci. Technol. **4**, 040502 (2019).

[29] K. Bongs, V. Boyer, M. Cruise, A. Freise, M. Holynski, J. Hughes, A. Kaushik, Y.-H. Lien, A. Niggebaum, M. Perea-Ortiz *et al.*, The UK national quantum technologies hub in sensors and metrology (keynote paper), Proc. SPIE **9900**, 990009 (2016).

[30] S. H. Madkhaly, L. A. Coles, C. Morley, C. D. Colquhoun, T. M. Fromhold, N. Cooper, and L. Hackermüller, Performance-optimized components for quantum technologies via additive manufacturing, PRX Quantum **2**, 030326 (2021).

[31] S. Madkhaly, N. Cooper, L. Coles, and L. Hackermüller, High-performance, additively-manufactured atomic spectroscopy apparatus for portable quantum technologies, Opt. Express **30**, 25753 (2022).

[32] S. Losev, D. Sevostianov, V. Vassiliev, and V. Velishansky, Production of miniature glass cells with rubidium for chip scale atomic clock, Phys. Procedia **71**, 242 (2015).

[33] Y. Ji, J. Shang, G. Li, J. Zhang, and J. Zhang, Microfabricated shaped rubidium vapor cell for miniaturized atomic magnetometers, IEEE Sens. Lett. **4**, 2500104 (2020).

[34] E. Talker, P. Arora, R. Zektzer, Y. Sebbag, M. Dikopltsev, and U. Levy, Light-Induced Atomic Desorption in Microfabricated Vapor Cells for Demonstrating Quantum Optical Applications, Phys. Rev. Appl. **15**, L051001 (2021).

[35] V. G. Lucivero, A. Zanoni, G. Corrielli, R. Osellame, and M. W. Mitchell, Laser-written vapor cells for chip-scale atomic sensing and spectroscopy, Opt. Express **30**, 27149 (2022).

[36] O. Schmidt, K.-M. Knaak, R. Wynands, and D. Meschede, Cesium saturation spectroscopy revisited: How to reverse peaks and observe narrow resonances, Appl. Phys. B **59**, 167 (1994).

[37] N. Cooper and T. Freegarde, Trapping of ^{85}Rb atoms by optical pumping between metastable hyperfine states, J. Phys. B **46**, 215003 (2013).

[38] D. A. Steck, Alkali D line data, http://steck.us/alkalidata.

[39] Note that the cross section varies between atoms according to velocity and location and between the outward and return components of the light; the value given by (13) is an average over this distribution.

[40] Stabilization to exactly identical frequencies is not possible, as appropriate lock points do not exist in the conventional Doppler-free absorption spectra.

[41] S. Utreja, H. Rathore, M. Das, and S. Panja, Frequency stabilization of multiple lasers to a reference atomic transition of Rb, Sci. Rep. **12**, 20624 (2022).

[42] A. Strangfeld, B. Wiegand, J. Kluge, M. Schoch, and M. Krutzik, Compact plug and play optical frequency reference device based on doppler-free spectroscopy of rubidium vapor, Opt. Express **30**, 12039 (2022).

[43] A. Gusching, M. Petersen, N. Passilly, D. Brazhnikov, M. Hafiz, and R. Boudot, Short-term stability of Cs microcell-stabilized lasers using dual-frequency sub-doppler spectroscopy, J. Opt. Soc. Am. B **38**, 3254 (2021).

[44] V. Maurice, C. Carlé, S. Keshavarzi, R. Chutani, S. Queste, L. Gauthier-Manuel, J. Cote, R. Vicarini, M. Abdel Hafiz, R. Boudot, and N. Passilly, Wafer-level vapor cells filled with laser-actuated hermetic seals for integrated atomic devices, Microsyst. Nanoeng. **8**, 129 (2022).

[45] D. McCarron, S. King, and S. Cornish, Modulation transfer spectroscopy in atomic rubidium, Meas. Sci. Technol. **19**, 105601 (2008).